Sliding Mode Sensorless Control of PM Synchronous Motor for Direct-Driven Washing Machines

Song Chi, Student Member, Longya Xu, Fellow IEEE
Dept. of Electrical and Computer Engineering
The Ohio State University
2015 Neil Avenue
Columbus, OH 43210 USA
chi.36@osu.edu, xu.12@osu.edu

Zheng Zhang, Senior Member, IEEE
Research & Engineering Center
Whirlpool Corporation
750 Monte Road MD: 5210
Benton Harbor, MI 49022
zheng_zhang@whirlpool.com

***Abstract*— The rotor position of PMSM is estimated by a novel sliding mode observer (SMO) operating over a wide speed range including deep flux-weakening region. By properly selecting equivalent control feedback gains, the estimation error of rotor position is reduced in low speeds and fast convergence of SMO guaranteed in high speeds. Compared to other PMSM systems for direct-driven washers using Hall Effect sensors, the control scheme features high torque production and fast dynamic response, especially in the deep flux weakening high-speed range. The sensorless control algorithm is robust to the armature reaction that seriously affects Hall Effect sensor signals and degrades torque production. The proposed sensorless control algorithm is verified by both computer simulation and experimental testing with a dynamometer as well as a direct-driven washer.**

Keywords- sensorless; direct driven; sliding mode observer; wide speed range, washing machine

I. INTRODUCTION

In recent years, direct drive systems have been increasingly applied in domestic washing machines due to their high efficiency and reliability as well as low noise and vibration. By this technology, the tub or drum of a washing machine is directly coupled to the motor shaft without transmission assembly which includes clutches, pulleys and/or gearboxes. This compact configuration results in the elimination of the breakage risk of the belt and reduction of energy losses. As well known, permanent magnet synchronous motors (PMSM) have many advantages such as the high power density, torque to inertia ratio and energy efficiency, which make them attractive candidates for the direct drive systems. Such kind of direct drive systems normally requires a high starting torque and wide speed range. In order to satisfy these requirements, the PMSMs are operated not only in the constant torque region when the speed is below the base speed but also in the constant power region with deep flux weakening over a wide high speed range. Recently, the continuous cost reduction of magnetic materials with high energy density and coercitivity, such as samarium cobalt and neodymium-boron iron, has opened up new possibilities for large-scale applications of PMSM and a continuous increase in cost-effective PM appliance drive systems will be witnessed in the near future [1, 2].

Normally low-cost Hall Effect sensors are used to provide rotor position feedback for the closed-loop motion control of PMSM in home appliance products. Such PMSM drive systems can usually meet the torque speed requirements both in wash and rinse cycle for washing machines. However, the six-step rectangular currents fed to the PMSM can cause large torque ripple and degrade system performance. To reduce torque ripple in the PMSM drive systems using Hall Effect sensors, several methods have been proposed [3, 4]. The most common one is to estimate the rotor position angle by integrating its speed every 60 electrical degrees. Conventional vector control using sine-shape current can then be implemented using the estimated rotor position angle. As a result of using sinusoidal currents, a smooth torque is produced. Unfortunately there inevitably exist measurement errors of Hall Effect sensor signals caused by armature reaction effects and limitations of installation [5]. The physical tolerance of Hall Effect sensors may generate significant errors in high speeds when vibration is large. Besides, the resolution of estimation is relatively low due to the only six updates per electrical cycle. Furthermore, the resultant rotor position measurement error can cause reduced maximum torque production and speed jitter especially in the high-speed flux-weakening region.

In order to further cut the hardware costs as well as improve the speed control performance and robustness to disturbances, many research efforts have been made to develop position sensorless control algorithms [6-10]. An iterative sliding-mode observer was presented to reduce the chattering components superimposed on the estimated back-EMF [9]. The presented sensorless control was implemented by iterating the calculation of observer recursively several times within a current sampling period in high speeds. Obviously this method increases the burden of computation to the hardware. On the other hand, no improvement could actually be made in low speeds. For improvement, a state filter was proposed in [10] for estimating the saliency-based back-EMF of PMSM in the rotor reference frame. Two PI controllers were used to estimate the rotor position angle and speed. Essentially, this method requires the knowledge of accurate system parameters. In addition, it is quite challenging to tune the PI controllers and make the estimated signals less affected by the bandwidth of the state filter and the rotating rotor frequency over a wide speed range.

This paper presents a position sensorless vector control scheme of PMSM for direct-driven domestic washing machines based on sliding mode theory. A novel sliding mode observer is proposed for estimation of the rotor position angle over a wide speed range including deep flux-weakening region. A feedback of equivalent control is proposed and investigated. By this method the estimation error can be reduced in the low-speed range and fast convergence guaranteed in the high-speed range. The proposed control algorithm is implemented in a fully digital speed control system based on a digital signal processor (DSP). Comparison of torque production between the proposed sliding mode sensorless scheme and the Hall Effect sensor based vector control is conducted. In particular, the estimation performance of rotor position and control robustness with respect to disturbances from load and dc bus voltage are examined. To verify the proposed estimation and control methods, an experimental setup of PMSM drive system is designed and built. Experimental results are presented to prove the feasibility of the proposed scheme.

II. POSITION SENSORLESS CONTROL OF PMSM

A. Mathematical Model of PMSM in the Stationary Reference Frame

The dynamic equations of a PMSM without saliency in the stationary reference frame can be expressed in the matrix form as

$$\dot{\vec{i}}_s = A \cdot \vec{i}_s + B \cdot (\vec{v}_s - \vec{e}_s) \tag{1}$$

$$\text{where} \quad A = \begin{bmatrix} -R_s/L_s & 0 \\ 0 & -R_s/L_s \end{bmatrix} \qquad B = \begin{bmatrix} 1/L_s & 0 \\ 0 & 1/L_s \end{bmatrix}$$

$$\vec{i}_s = \begin{bmatrix} i_{\alpha s} \\ i_{\beta s} \end{bmatrix} \qquad \vec{v}_s = \begin{bmatrix} v_{\alpha s} \\ v_{\beta s} \end{bmatrix}$$

$$\vec{e}_s = \begin{bmatrix} e_{\alpha s} \\ e_{\beta s} \end{bmatrix} = K_e \cdot \omega_r \cdot \begin{bmatrix} -\sin(\theta_r) \\ \cos(\theta_r) \end{bmatrix}$$

L_s, R_s and K_e refer to the stator inductance, resistance and back-EMF constant.

B. Sliding Mode Observer

The sliding mode observer (SMO) is designed as

$$\dot{\hat{\vec{i}}}_s = A \cdot \hat{\vec{i}}_s + B \cdot (\vec{v}^{\,*}_s + l \cdot \vec{Z}_{eq} + \vec{Z}) \tag{2}$$

$$\vec{Z} = -K \cdot sign\ (\hat{\vec{i}}_s - \vec{i}_s)$$

$$l = \begin{cases} -0.5 & (n < 180\ rpm) \\ 1 & (n \geq 180\ rpm) \end{cases}$$

$$\text{where} \quad K = \begin{bmatrix} k & 0 \\ 0 & k \end{bmatrix}$$

$$\vec{i}_s = \begin{bmatrix} i_{\alpha s} \\ i_{\beta s} \end{bmatrix} \qquad \vec{v}^{\,*}_s = \begin{bmatrix} v^*_{\alpha s} \\ v^*_{\beta s} \end{bmatrix} \qquad \hat{\vec{i}}_s = \begin{bmatrix} \hat{i}_{\alpha s} \\ \hat{i}_{\beta s} \end{bmatrix}$$

$$sign\ (\hat{\vec{i}}_s - \vec{i}_s) = \begin{bmatrix} sign\ (\hat{i}_{\alpha s} - i_{\alpha s}) \\ sign\ (\hat{i}_{\beta s} - i_{\beta s}) \end{bmatrix}$$

In (2), l is the feedback gain of the equivalent control Z_{eq}, and k, normally positive (k>0), is the switching gain of the discontinuous control Z. The superscript '*' indicates a command variable. Matrix A and B are defined in (1).

The equivalent control Z_{eq} can be obtained as

$$\vec{Z}_{eq} = \begin{bmatrix} Z_{eq\alpha} \\ Z_{eq\beta} \end{bmatrix} = \begin{bmatrix} -k \cdot sign(\hat{i}_{\alpha s} - i_{\alpha s}) \cdot \dfrac{\omega_c}{s+\omega_c} \\ -k \cdot sign(\hat{i}_{\beta s} - i_{\beta s}) \cdot \dfrac{\omega_c}{s+\omega_c} \end{bmatrix}. \tag{3}$$

$$\omega_c : \quad freq\_cutoff$$

A low-pass filter is used in (3). It is noticed that its cutoff frequency should be designed properly with respect to the fundamental frequency of the PMSM currents.

Fig. 1 shows a block diagram of the proposed sliding mode observer.

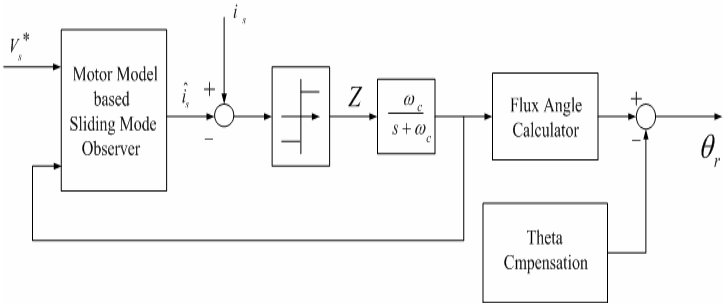

Figure 1. Block diagram of the proposed sliding mode observer

To solve the chattering problem, the sign function is replaced by a saturation function as shown in Fig. 2. When the magnitude of current error is less than E_0, the control Z changes to a saturation function as

$$\vec{Z} = -k_s \cdot (\hat{\vec{i}}_s - \vec{i}_s) \tag{4}$$

where $k_s = k / E_0$.

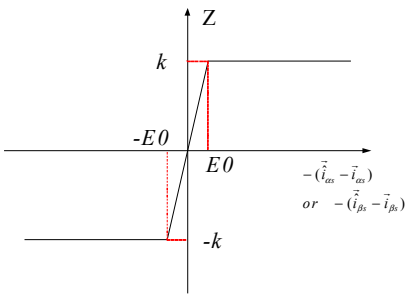

Figure 2. Diagram of the saturation function

Considering (1) and (2), we can obtain the dynamic sliding mode motion equation as expressed in

$$\dot{S} = A \cdot S + B \cdot (\vec{e}_s + l \cdot \vec{Z}_{eq} + \vec{Z}) \quad \text{where} \quad S = \hat{\vec{i}}_s - \vec{i}_s \tag{5}$$

If the switching gain of Z, k, is large enough to guarantee the following

$$\dot{S}^T \cdot S < 0 \tag{6}$$

then sliding mode will exist and we get

$$\vec{e} = \begin{bmatrix} e_{\alpha s} \\ e_{\beta s} \end{bmatrix} = -(1+l)\vec{Z}_{eq} \cdot \tag{7}$$

Furthermore, the rotor position angle $\hat{\theta}_r$ can be estimated by using the equivalent control Z_{eq} as follows.

$$\hat{\theta}_r = -\tan^{-1}(\frac{\hat{e}_{s\alpha}}{\hat{e}_{s\beta}}) = -\tan^{-1}(\frac{Z_{eq\alpha}}{Z_{eq\beta}}) \cdot \tag{8}$$

It is noticed that the estimated rotor position angle $\hat{\theta}_r$ should be added by π when the rotation direction is reversed.

From (7), we can see that the magnitude of the equivalent control Z_{eq} is two times larger than that of the back-EMF with l = -0.5. The rotor position of PMSM is calculated from Z_{eq}. Although the back-EMF is small in low speeds, the estimated Z_{eq} is enlarged. Therefore, with the same quantization limits in the real-time implementation, the proposed observer is able to work at lower speeds and improve the quality of the estimated rotor position angle, or equivalently to extend the minimum operating speed.

By substituting (4) into (5), we get

$$\dot{S} = \left[A - (l+1) \cdot k_s \cdot B\right] \cdot S + B \cdot \vec{e}_s \tag{9}$$

Direct examination of the above shows the system trajectories are firstly guaranteed to converge to the boundary layer, i.e. a small E_0-vicinity of the origin. Because the system is continuous and linear within the boundary layer, the eigenvalue placement is achieved by setting l = 1 to accelerate the convergence rate of SMO in high speeds and guarantee further convergence to zero. Hence, the invariance property of sliding mode control is partially preserved in the sense that the system trajectories are confined to a vicinity of the sliding manifold $S(t)$=0, instead of exactly to $S(t)$=0 as in ideal sliding mode [11]. Within the vicinity, the system behavior of further convergence to zero is guaranteed. It can be seen that the eigenvalues of $A-(l+1)\cdot k_s \cdot B$ become smaller with l increasing, resulting in faster convergence rate of $S(t)$ to zero that is critical to the high-speed operation.

III. Overall Control System

Fig. 3 shows a block diagram of the overall control system, which consists of a speed PI regulator, a flux-weakening controller, two current PI regulators in the synchronous reference frame, a speed calculator implemented by a Phase-Locked Loop (PLL) and a rotor position estimator by the sliding mode observer. In addition, the conventional modules for vector control such as Clark, Park and inverse Park transformation, space vector PWM generation module, a 3-phase power inverter and the PMSM are included. When the speed of the PMSM is above its base speed, the flux-weakening controller will be activated, which generates the required demagnetizing current command for the flux-weakening operation.

Near standstill, the back-EMF of the PMSM is too small to be estimated accurately. Therefore, an open-loop starting algorithm with a ramp speed command profile is designed to kick off the motor from standstill and accelerate it up to a specific speed, i.e. 25rpm, at which the proposed sliding mode observer is activated. A relatively smooth start can be achieved by this method and considered adequate for startup without fast acceleration.

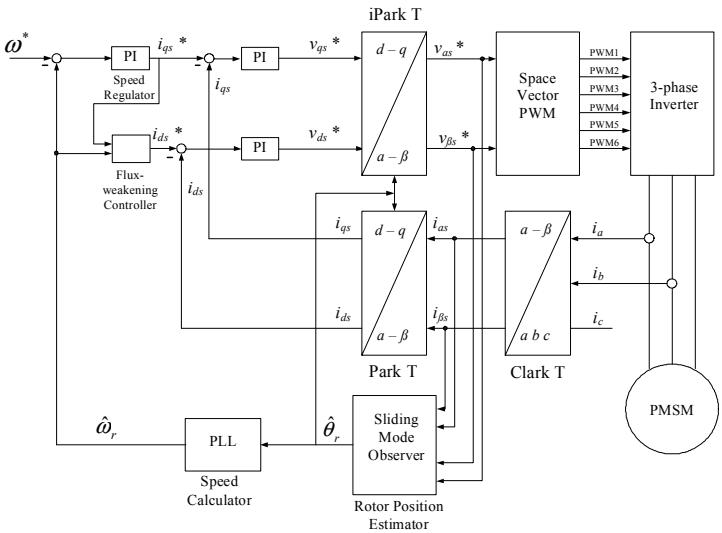

Figure 3. Block diagram of overall control system

IV. SIMULATION AND EXPERIMENTAL RESULTS

A. Simulation results

The proposed position sensorless control algorithm based on the sliding mode observer has been simulated by Simulink/MatLab. The parameters of PMSM are: R_s = 16 ohm, L_s = 60 mH and K_e = 0.22 Vs/rad. The base speed is 250 rpm. The dc bus voltage of the power inverter is 310V. The space vector PWM algorithm is applied and updated every 50 μs with respect to the switching frequency of 20kHz. Variables in the speed and current regulators are in per unit. The speed base is chosen to be 1250 rpm and current base 7A. The switching gain k of the sliding mode observer is 800. The cutoff frequency of the low-pass filter for obtaining the equivalent control is 4000π rad/s while the maximum fundamental frequency of current is1000π rad/s.

Fig.4 shows the simulation results when the motor was running at 50rpm with l = -0.5 in (a) and at 1000rpm with l = 1 in (b). In the two cases, actual and estimated waveforms of both rotor position angle and stator current almost overlap together with very small errors (much smaller than 0.01). In the figure, 0.01 of angle error represents 0.57 electrical degree. In addition, the control Z_a was sampled in real time at minimum frequency of 1 GHz. Other signals were sampled at fixed 100 kHz. It is noticed that Z_a is not aligned with other signals in time and plotted in sample dots.

Fig.5 shows the robustness of the system with respect to the disturbances from load and dc bus voltage. In the simulation the motor was accelerated from 0 to 500 RPM. The dc bus voltage was initially 310 V and ramped to 320 V in 2s. and then down from 320V to 280V. The load was initially 0 Nm and stepped to 1 Nm. in 2.5s. We can observe that the speed error is much less than 0.001 in per unit, which refers to 1.25rpm at 500rpm in both steady state and transient in the flux-weakening region.

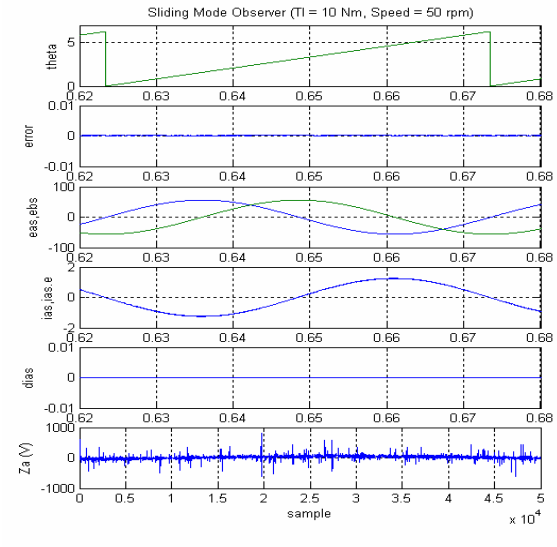

(a)

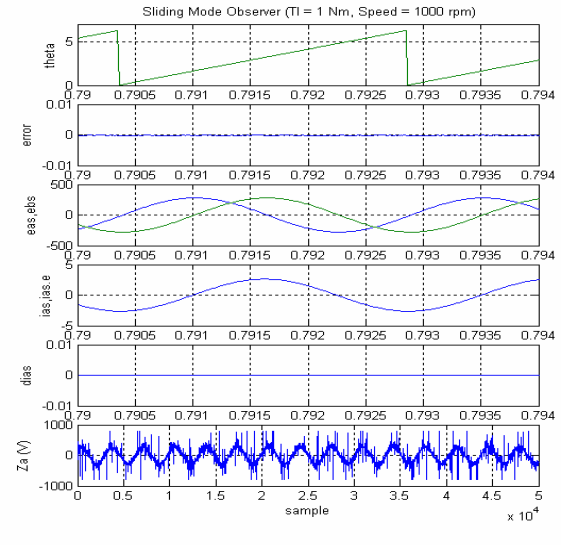

(b)

Figure 4. Actual and estimated angle (up) and estimation error (2nd), estimated back-EMF (3rd), measured and estimated current i_{qs} (4th) and error (5th), and sliding mode control Za (bottom) (a) l=-0.5 @50rpm, (b) l=1@1000rpm

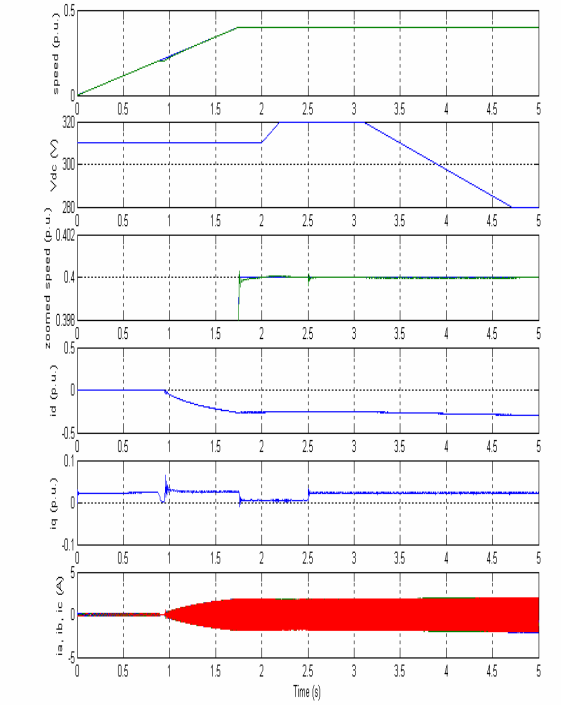

Figure 5. Speed command and feedback (up), V_{dc} (2nd), zoomed speed command and feedback (3rd), i_{ds} (4th), i_{qs} (5th) and stator phase current i_{as} (5.0 A/div, bottom)

B. Experimental results

An experimental PMSM drive system has been set up to verify the proposed sensorless control, which includs: 1) a 48-pole non-saliency outer-rotor PMSM with its base speed of 250 rpm, 2) a DSP controller, 3) a three-phase power inverter and 4) a dynamometer coupled with the shaft of the PMSM as load. The switching frequency of power inverter is 20kHz. Space vector PWM is used for the PWM generation. The dc bus voltage of the power inverter is 310V and the maximum current 7A. The sampling frequency of the current and voltage measurement is also 20 kHz. The parameters of PMSM are: R_s=16 ohm, L_s=60 mH and K_e=0.22 Vs/rad, same as in the computer simulation.

Moreover, a direct drive washer was used to verify the proposed the control algorithm. The motors in the experimental drive system and the washer were identical.

In Figs. 6 and 7, the real rotor position is measured by the encoder ($\theta_{encoder}$) and the estimated one ($\hat{\theta}_{SMO}$) by the proposed sliding mode observer. Hall Effect sensor signal *Hall_A* and phase current i_a and i_b are also displayed.

Figs.6 shows the experimental results when the motor was running at 50 rpm (20% base speed) with a constant load of 10 Nm (30% maximum torque) and Fig.7 at 1000 rpm (400% base speed) with a constant load of 1 Nm (50% available maximum torque according to speed). We can see the well-behaved rotor position estimation from the SMO observer and the well-regulated sinusoidal current waveforms. The estimated angle $\hat{\theta}_{SMO}$ aligns with $\theta_{encoder}$ and *Hall_A* well. It indicates that the estimation error of the rotor position angle is very small resulting in low harmonics on the phase currents and high efficiency. The output rotor position signals in Fig. 7 are rounded on the bottom corner due to the limited bandwidth of monitor circuits.

Figs.8 through 10 show the transient response when the motor was running at 50, 500 and 1000 rpm with step-on and -off load of 10 Nm, 5 Nm and 2 Nm respectively. As observed, the speed is well regulated over a wide range regardless of load disturbance.

Fig. 11 shows the comparison of maximum available torque with respect to operating speeds between the Hall- and proposed sensorless SMO-based algorithm. Experiments were carried out on identical PMSMs. It can be seen that more torque is produced by the proposed senseless algorithm in the high-speed range, especially 10% more at 500 and 1000 rpm.

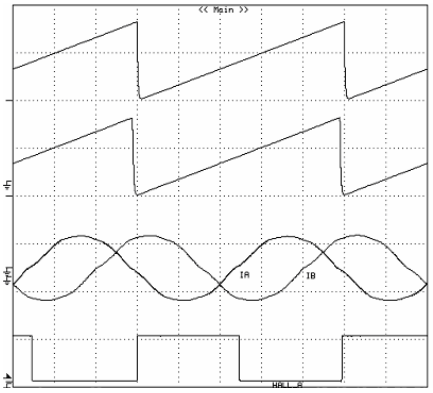

Figure 6. Rotor position angle $\theta_{encoder}$ (up), $\hat{\theta}_{SMO}$ (2nd), i_a and i_b (1.0 A/div, 3rd) and *Hall_A* (bottom) 10ms/div

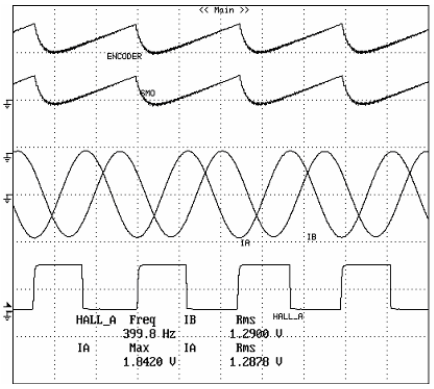

Figure 7. Rotor position angle $\theta_{encoder}$ (up), $\hat{\theta}_{SMO}$ (2nd), i_a and i_b (2.0 A/div, 3rd) and *Hall_A* (bottom) 1ms/div

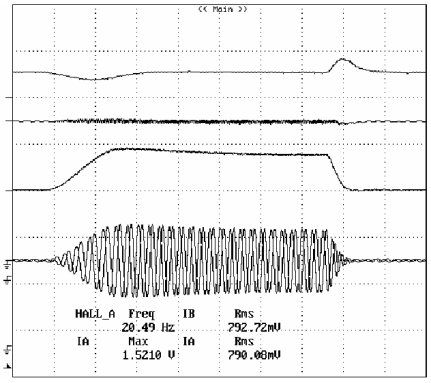

Figure 8. Rotor speed $n_{encoder}$ (*75 rpm/div*, up), i_{ds} (*1.7A/div*, 2nd), i_{qs} (*1.7A/div*, 3rd) and i_a and i_b (2.0 A/div, bottom) 200ms/div

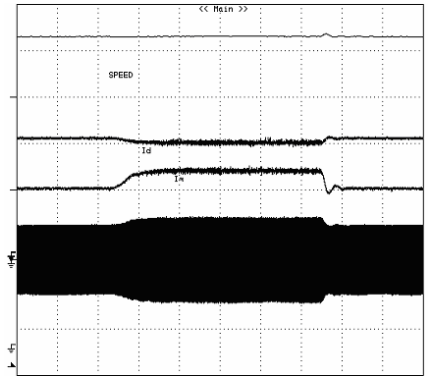

Figure 9. Rotor speed $n_{encoder}$ (*380 rpm/div*, up), i_{ds} (*1.7A/div*, 2nd), i_{qs} (*1.7A/div*, 3rd) and i_a and i_b (2.0 A/div, bottom) 500ms/div

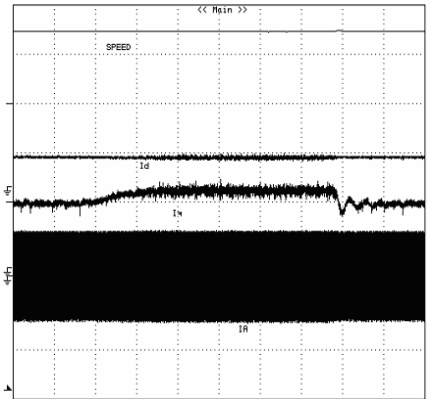

Figure 10. Rotor speed $n_{encoder}$ (*757 rpm/div*, up), i_{ds} (*1.7A/div*, 2nd), i_{qs} (*1.7A/div*, 3rd) and i_a and i_b (2.0 A/div, bottom) 500ms/div

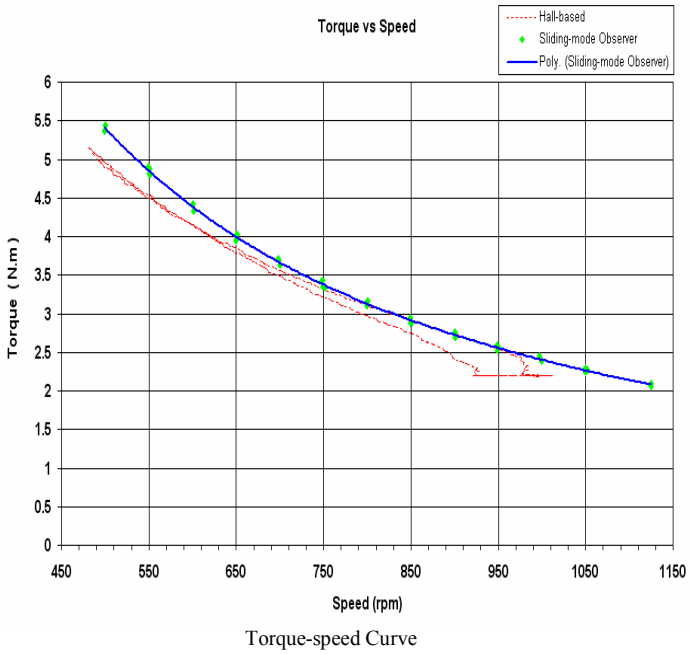

Torque-speed Curve

Figure 11. Comparison between Hall- and sensorless SMO –based control algorithm

Figs.12 and 13 show the washer testing results when the drum is loaded with 1.0kg rubber. The washer drum was spun between –75rpm and +75rpm back and forth to simulate the operation of washing agitation cycle. The estimated rotor position angle, speed command and feedback, and the measured phase current i_{as} are shown in Fig 12 respectively. As expected, the drum speed tracks the ramp speed command profile both in the open-loop starting and after transition to the closed-loop sensorless control. Larger phase current can be seen close to zero speed than that after the transition, which guarantees the reliable low-speed operation.

In Fig.13, the speed command and feedback, current i_{ds} and i_{qs}, and phase current i_{as} are shown when the drum was accelerated from 50 to 1025 rpm and stayed thereafter to simulate the operation of rinse spin cycle. The dc bus voltage varied between 320V and 280V. The onset of flux-weakening control was set at 180 rpm. We can observe the automatically generated demagnetizing current i_{ds} and the speed control performance within the whole speed range including the deep flux-weakening region.

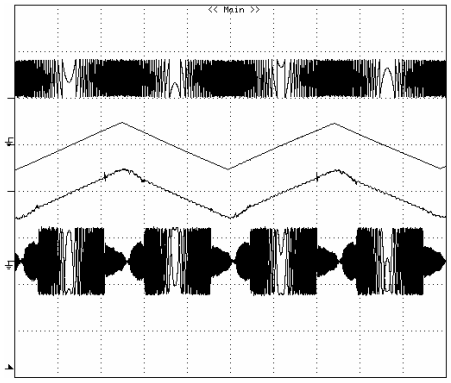

Figure 12. Estimated rotor position angle $\hat{\theta}_{SMO}$ (up), speed command (150 rpm/div, 2nd), real speed (150 rpm/div, 3rd), and measured current i_{as} (1.0 A/div, bottom) 2s/div

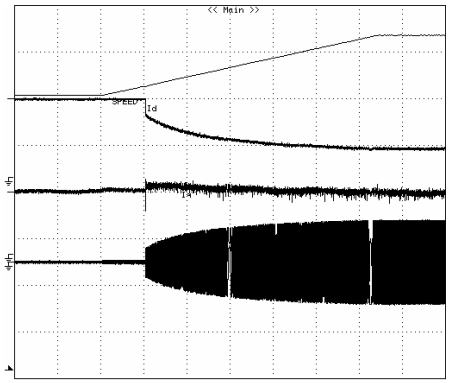

Figure 13. Speed command and feedback (757 rpm/div, up), i_{ds} (1.7 A/div, 2nd), i_{qs} (1.7 A/div, 3rd) and stator phase current i_{as} (1.0 A/div, bottom), 10s/div

All the experimental and washer testing results indicate that the proposed sensorless control algorithm is valid and the real-time implementation is successful.

V. CONCLUSIONS

In this paper, a position sensorless vector control scheme of PMSM for domestic direct-driven washing machines is presented. A novel sliding mode observer has been developed for the estimation of rotor position angle over a wide speed range including deep flux-weakening region. A feedback of equivalent control results in small estimation error in the low-speed range and fast convergence in the high-speed range, which is critical to high-speed operation. The proposed control algorithm has been successfully implemented in real time. The estimation performance of rotor position angle and control robustness have been demonstrated. Compared to other PMSM drive systems using Hall Effect sensors, the control scheme achieves higher torque production. The feasibility of the proposed sensorless control scheme has been verified by both computer simulation and experimental results

ACKNOWLEDGMENT

This work was supported by the Research and Engineering Center of Whirlpool.

REFERENCES

[1] T. Tanaka, "Environment friendly revolution in home appliances," in proceedings of *ISPSD'*, 2001, pp. 91–95.

[2] K. Y. Cho and C. H. Hong, "Sensorless control of a PM synchronous motor for direct drive washer without rotor position sensors," *IEE Proc-Electr. Power Appl.,* vol. 151, No. 1, pp. 61-69, Jan. 2004.

[3] T. D. Batzel and K. Y. Lee, "Commutation torque ripple minimization for permanent magnet synchronous machines with Hall effect position feedback," *IEEE Trans. Energy Conv.,* vol. 13, pp. 257-262, Sep. 1998.

[4] J. Bu, L. Xu and et al, "Near-zero speed performance enhancement of PM synchronous machines assisted by low-cost Hall effect sensors," in *Conf. Rec.IEEE- APEC'98*, vol. 1, 1998, pp. 64–68.

[5] Z. Xu, K. T. Li, Y. Lu and B. Guo, "Position-measuring error analysis and solution of Hall sensor in pseudo-sensorless PMSM driving system," in *IECON Annu. Conference Record*, vol. 2, 2003, pp. 1337–1342.

[6] Z. Yan and V. Utkin, "Sliding mode observers for electric machines-an overview," in *Conf. Rec. IEEE-IES 28th Annu. Meeting IECON02*, vol. 3, 2002, pp. 1842–1847.

[7] Z. M. Peixoto, et al., "Speed control of permanent magnet motors using sliding mode observers for induced emf, position and speed estimation," in *Conf. Rec. IEEE-IAS Annu. Meeting*, vol. 2, 1995, pp. 1023–1028.

[8] Z. Zhang, H. Xu, L. Xu and L. E. Heilman, "Sensorless direct field-oriented control of three-phase induction motors based on "Sliding Mode" for washing-machine drive applications," *IEEE Trans. Ind. Applt.*, vol. 42, pp. 694-701, May/June 2006.

[9] K. Kang, J. Kim and et al, "Sensorless control of PMSM in high speed range with iterative sliding mode observer," in *Conf. Rec.IEEE-APEC'04*, vol. 2, 2004, pp. 1111–1116.

[10] H. Kim, S. Yi, N. Kim and R. D. Lorenz, "Using low resolution position sensors in bumpless position/speed estimation methods for low cost PMSM drives," in *Conf. Rec. IEEE-IAS Annu. Meeting*, vol. 4, 2005, pp. 25186-2525.

[11] Vadim Utkin, J. Guldner and Jingxin Shi, "Sliding mode control in electromechanical systems," chap. 8, 1st Edition, Taylor&Francis, 1999.